Science
AAAS

Two-Color Single-Photon Photoinitiation and Photoinhibition for Subdiffraction Photolithography

Timothy F. Scott, *et al.*

Science **324**, 913 (2009);
DOI: 10.1126/science.1167610

Science (print ISSN 0036-8075; online ISSN 1095-9203) is published weekly, except the last week in December, by the American Association for the Advancement of Science, 1200 New York Avenue NW, Washington, DC 20005.

that is considerably longer than the 13-ns repetition time of our laser system. So long as the radicals do not diffuse apart, absorption of a photon from the deactivation beam can lead to back-transfer of the electron, depleting the radicals before they can react. If the radicals do diffuse apart, deactivation can no longer occur, accounting for the nondeactivatable channel.

With the phase mask used here, RAPID lithography can clearly produce features with heights as small as λ/20 along the optical axis. Analogous with results from STED microscopy, comparable transverse resolution should be attainable by employing a different phase mask, such as a spiral phase element (*24*). By using two phase-masked deactivation beams (*25*), it should further be possible to attain this resolution in all dimensions. The use of shorter excitation and deactivation wavelengths should improve resolution further. A current limiting factor in the resolution attainable is that even a CW deactivation beam can cause polymerization at high enough intensity. Because the resolution enhancement of RAPID lithography is based on an optical saturation effect, making the deactivation process more efficient should lead to finer features. In principle, the resolution of RAPID will ultimately be limited by material properties, particularly the minimum size of a self-supporting polymer voxel. With this limitation in mind, we believe that resolution on the order of 10 nm can be attained through full optimization of the photoresist properties and the optical configuration. Resolution on this scale may be attractive for next-generation lithography, particularly considering that RAPID lithography can be implemented with a table-top instrument.

References and Notes

1. S. E. Thompson, S. Parthasarathy, *Mater. Today* **9**, 20 (2006).
2. H. Ito, in *Microlithography: Molecular Imprinting* (Springer-Verlag, Berlin, 2005), vol. 172, *Advances in Polymer Science*, pp. 37–245.
3. S. Kawata, H. B. Sun, T. Tanaka, K. Takada, *Nature* **412**, 697 (2001).
4. M. Rumi, S. Barlow, J. Wang, J. W. Perry, S. R. Marder, in *Photoresponsive Polymers I* (Springer-Verlag, Berlin, 2008), vol. 213, *Advances in Polymer Science*, pp. 1–95.
5. C. N. LaFratta, J. T. Fourkas, T. Baldacchini, R. A. Farrer, *Angew. Chem. Int. Ed.* **46**, 6238 (2007).
6. D. Yang, S. J. Jhaveri, C. K. Ober, *Mater. Res. Sci. Bull.* **30**, 976 (2005).
7. J.-F. Xing *et al.*, *Appl. Phys. Lett.* **90**, 131106 (2007).
8. D. Tan *et al.*, *Appl. Phys. Lett.* **90**, 071106 (2007).
9. W. Haske *et al.*, *Opt. Express* **15**, 3426 (2007).
10. H.-B. Sun, T. Tanaka, S. Kawata, *Appl. Phys. Lett.* **80**, 3673 (2002).
11. T. A. Klar, S. Jakobs, M. Dyba, A. Egner, S. W. Hell, *Proc. Natl. Acad. Sci. U.S.A.* **97**, 8206 (2000).
12. S. W. Hell, *Science* **316**, 1153 (2007).
13. S. W. Hell, *Nat. Methods* **6**, 24 (2009).
14. C. S. Colley *et al.*, *J. Am. Chem. Soc.* **124**, 14952 (2002).
15. J. O. Hirschfelder, C. F. Curtiss, R. B. Bird, *Molecular Theory of Gases and Liquids* (Wiley, New York, 1954).
16. Materials and methods are available as supporting material on *Science* Online.
17. The maximum delay time of 13 ns is determined by the 76 MHz laser repetition rate.
18. Because MAIL from gold nanoparticles is a three-photon process at 800 nm, the images show the cubes of the PSFs.
19. R. A. Farrer, F. L. Butterfield, V. W. Chen, J. T. Fourkas, *Nano Lett.* **5**, 1139 (2005).
20. The deactivation laser was operated in fs pulsed mode for the purpose of measuring its PSF using MAIL but was operated in CW mode for all other experiments. The beam profile and direction did not change measurably in going from pulsed to CW mode, so we expect the PSF to be nearly identical in both modes.
21. All powers were as measured at the sample position.
22. The slight asymmetry of the voxel is due to our use of linearly polarized light for fabrication. See (*26*).
23. AFM cannot measure reentrant (overhanging) features, so although the voxels appear to be tapered in these images, they are not.
24. M. W. Beijersbergen, R. P. C. Coerwinkel, M. Kristensen, J. P. Woerdman, *Opt. Commun.* **112**, 321 (1994).
25. B. Harke, C. K. Ullal, J. Keller, S. W. Hell, *Nano Lett.* **8**, 1309 (2008).
26. H. B. Sun *et al.*, *Appl. Phys. Lett.* **83**, 819 (2003).

27. We appreciate the support of the Maryland NanoCenter and its Nanoscale Imaging, Spectroscopy, and Properties Laboratory (NISPLab). NISPLab is supported in part by NSF as a *Materials Research Science and Engineering Center* (MRSEC) Shared Experimental Facility. This work was supported in part by the UMD-NSF-MRSEC under grant DMR 05-20471. We are grateful to E. Williams for the use of her AFM and to J. Goldhar, Y. Leng, and V. Yun for fabricating the phase mask used in this work. The University of Maryland has filed a provision patent based on the work presented in this paper.

Supporting Online Material

www.sciencemag/org/cgi/content/full/1168996/DC1
Materials and Methods
SOM Text
Fig. S1
References

25 November 2008; accepted 19 March 2009
Published online 9 April 2009;
10.1126/science.1168996
Include this information when citing this paper.

Two-Color Single-Photon Photoinitiation and Photoinhibition for Subdiffraction Photolithography

Timothy F. Scott,[1]* Benjamin A. Kowalski,[2] Amy C. Sullivan,[2]† Christopher N. Bowman,[1] Robert R. McLeod[2]‡

Controlling and reducing the developed region initiated by photoexposure is one of the fundamental goals of optical lithography. Here, we demonstrate a two-color irradiation scheme whereby initiating species are generated by single-photon absorption at one wavelength while inhibiting species are generated by single-photon absorption at a second, independent wavelength. Co-irradiation at the second wavelength thus reduces the polymerization rate, delaying gelation of the material and facilitating enhanced spatial control over the polymerization. Appropriate overlapping of the two beams produces structures with both feature sizes and monomer conversions otherwise unobtainable with use of single- or two-photon absorption photopolymerization. Additionally, the generated inhibiting species rapidly recombine when irradiation with the second wavelength ceases, allowing for fast sequential exposures not limited by memory effects in the material and thus enabling fabrication of complex two- or three-dimensional structures.

Photopolymerizations typically proceed when a chromophore absorbs a photon and subsequently generates active centers that initiate the polymerization reaction. This single-photon process exhibits high irradiation sensitivity, enabling the use of low-power lasers and high writing speeds, which are critical for lithographic, stereolithographic, and data storage applications. However, feature size in depth is typically a multiple of the Rayleigh range of the focused beam (*1*), preventing the fabrication of micrometer-scale layers. Similarly, the transverse feature size is constrained by the diffraction limit, a physical property associated with the focusing power of lenses that is dependent on the wavelength of the incident light and the numerical aperture of the lens. Finer feature sizes are achieved by reducing the irradiation intensity or time (*2*); however, this procedure unavoidably reduces the contrast between the conversion of the gelled, insoluble material and the ungelled, soluble material and results in the fabrication of loosely cross-linked, mechanically unsound structures unable to withstand the rigors of solvent processing that are necessary for device fabrication.

These limitations are partially addressed by two-photon photopolymerization, wherein a chromophore absorbs two photons to initiate polymerization. This approach has been exploited by a number of researchers to realize the fabrication of three-dimensional (3D) nanostructures (*2*–*6*) with

[1]Department of Chemical and Biological Engineering, University of Colorado, Boulder, CO 80309–0424, USA. [2]Department of Electrical and Computer Engineering, University of Colorado, Boulder, CO 80309–0425, USA.

*Present address: Center for Bioengineering, Department of Mechanical Engineering, University of Colorado, Boulder, CO 80309–0427, USA.

†Present address: Department of Physics and Astronomy, Agnes Scott College, Decatur, GA 30030, USA.

‡To whom correspondence should be addressed. E-mail: robert.mcleod@colorado.edu

feature sizes below the diffraction limit. The premise of these studies is that two-photon absorption (and hence polymerization) only occurs efficiently near the center of the focal volume, where photon density is highest. For many initiators, however, the two-photon absorption cross section is inherently small. Several approaches have been exploited to address this issue, such as application of π-conjugated donor-acceptor compounds (*3*) and quantum dots (*7*) or use of photochromic compounds as two-photon photosensitizers in free-radical photopolymerizations (*8*–*11*). Unfortunately, many of the confinement benefits of two-photon processes are lost when the intermediate lifetime is greater than the exposure time. Moreover, high-power sources such as pulsed Ti:sapphire lasers focused in small areas are required for rapid exposures. Thus, only point exposures and low translation speeds are feasible. Ultimately, the combination of laser cost and extremely long fabrication times substantially decreases the scalability and impact of these processes.

An alternative means of confining polymerization would be to activate a localized inhibitor such as a radical trap transiently. Here, we describe a scheme whereby the initiation and the inhibition of a radical photopolymerization are uniquely correlated to two distinct irradiation wavelengths. Photoinduced inhibition is accomplished by noninitiating radicals produced via single-photon photolysis of an otherwise inert compound. These radicals are able to couple with the growing polymer chain, terminating polymerization and halting chain growth. Moreover, the inhibiting radicals are small molecular species that remain unbound to the polymer network and thus diffuse rapidly (*12*). As a result, they may be very short-lived, recombining with each other at

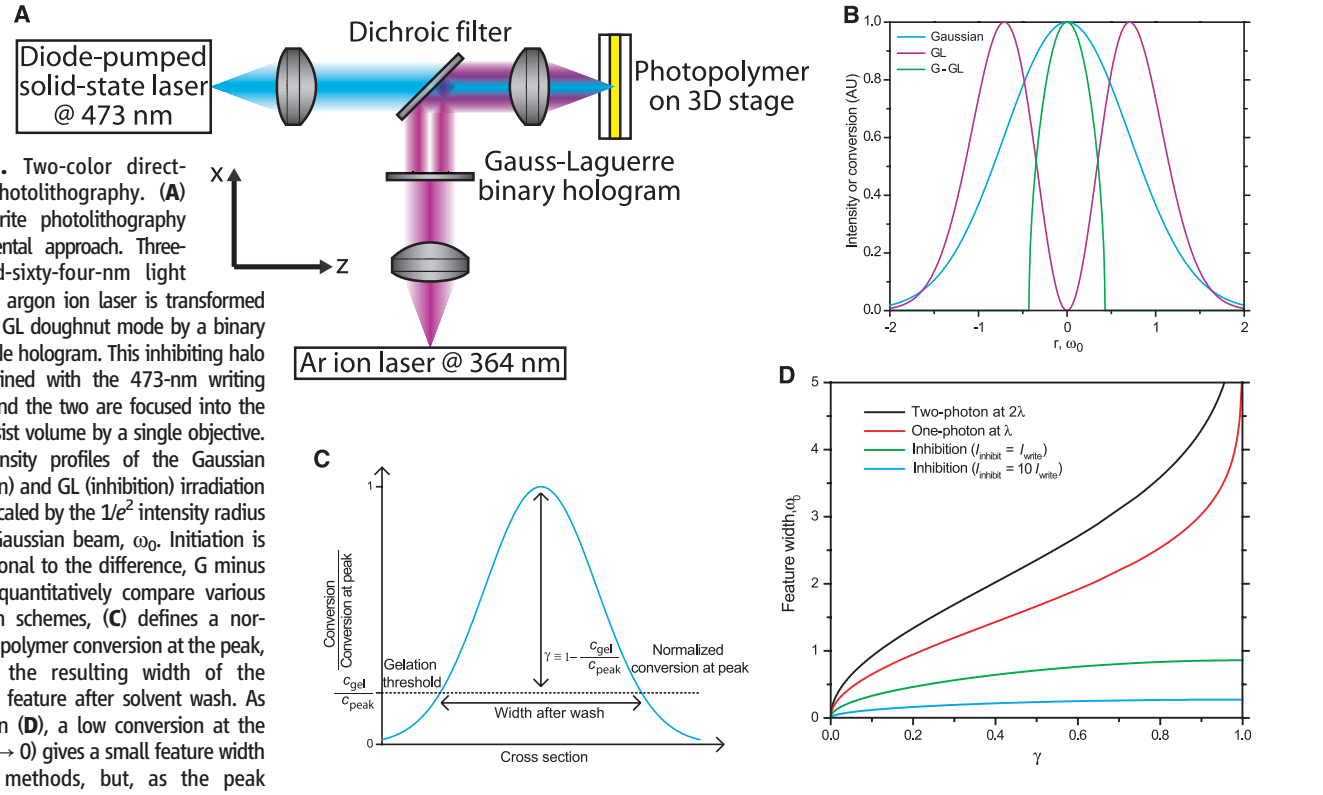

Fig. 1. Two-color direct-write photolithography. (**A**) Direct-write photolithography experimental approach. Three-hundred-sixty-four-nm light from an argon ion laser is transformed into the GL doughnut mode by a binary amplitude hologram. This inhibiting halo is combined with the 473-nm writing stylus, and the two are focused into the photoresist volume by a single objective. (**B**) Intensity profiles of the Gaussian (initiation) and GL (inhibition) irradiation modes scaled by the $1/e^2$ intensity radius of the Gaussian beam, ω_0. Initiation is proportional to the difference, G minus GL. To quantitatively compare various initiation schemes, (**C**) defines a normalized polymer conversion at the peak, γ, and the resulting width of the polymer feature after solvent wash. As shown in (**D**), a low conversion at the peak ($\gamma \to 0$) gives a small feature width for all methods, but, as the peak conversion is increased ($\gamma > 0$), one- and two-photon feature sizes rapidly increase. In contrast, the reported method maintains small feature sizes for arbitrary peak conversions. This feature size is independently adjusted by increasing the intensity of the inhibition wavelength.

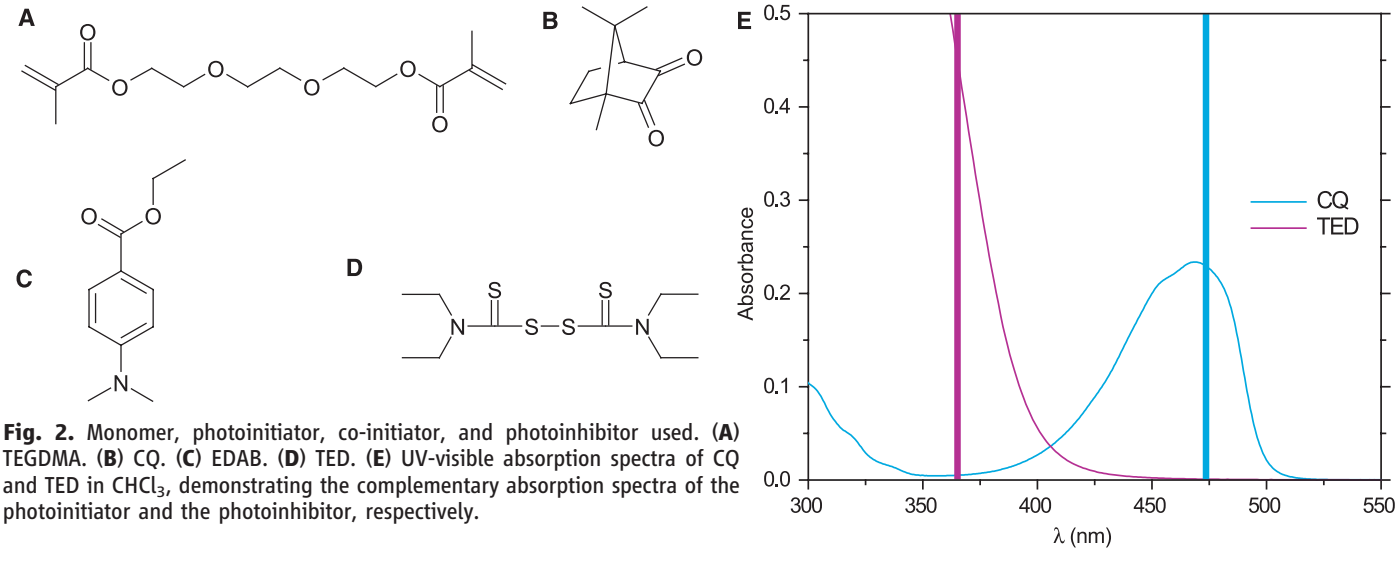

Fig. 2. Monomer, photoinitiator, co-initiator, and photoinhibitor used. (**A**) TEGDMA. (**B**) CQ. (**C**) EDAB. (**D**) TED. (**E**) UV-visible absorption spectra of CQ and TED in $CHCl_3$, demonstrating the complementary absorption spectra of the photoinitiator and the photoinhibitor, respectively.

diffusion-controlled rates so that their concentration falls precipitously in the absence of photolysing irradiation. Assuming all species formed in the recombination reactions are also inert, there should be negligible residual inhibiting species after the photolysing irradiation has ceased.

To implement this technique, we focused the photoinhibiting beam into a Gauss-Laguerre (GL) "doughnut" mode surrounding the focal point of the primary beam used to initiate polymerization. An analogous irradiation scheme used in stimulated emission-depletion (STED) microscopy has been shown to resolve features on the order of 15 nm (*13*). In a similar vein, the final polymerized feature size in this irradiation scheme is a function of the difference between initiation and inhibition patterns. Uniquely, this difference is not governed by the conventional diffraction limit as in traditional photolithography: The limit now is determined by the contrast that is maintained between initiation and inhibition. The small but finite initiation rate of the inhibiting radicals sets an upper limit on the ratio of inhibiting to initiating intensities, in turn limiting the confinement shown in Fig. 1D.

The layout of the optical system used to demonstrate this capability is shown in Fig. 1A (*14*). The initiating and inhibiting wavelengths are manipulated into complementary Gaussian and GL irradiation modes, respectively, where the GL mode is generated by a binary hologram. The GL mode is characterized by a central null, a high-contrast, topological feature of the electric field that is maintained throughout the entire focal volume. The two beams are combined with a dichroic filter and focused into the volume of the substrate material; the resulting diffraction-limited profiles at the coincident focal plane are shown in Fig. 1B. This two-color irradiation scheme produces a region of initiating species surrounded by a doughnut of inhibiting species.

The size of the resulting polymerized region is predicted by noting that, through application of the steady-state approximation (*15*), the polymerization rate (R_p) is predicted to scale with the square root of the initiation rate (R_i) for exclusively bimolecular termination. Thus, for single-photon absorption, R_i scales linearly with the irradiation intensity I and R_p is proportional to $I^{0.5}$. In the presence of photoinhibiting species, R_i is modified such that R_p scales as $(I_{blue} - \beta \times I_{UV})^{0.5}$, where I_{blue} and I_{UV} are the blue and ultraviolet (UV) irradiation intensities, respectively, and β is a constant encompassing the ratios of the inhibitor to the initiator absorption cross sections, quantum yields, and reaction rate constants. With this model, the predicted polymerization profile, shown in Fig. 1B for the case of $\max(I_{blue}) = \max(\beta \times I_{UV})$, is substantially smaller than the diffraction-limited spot size. Note that feature widths can be reduced by increasing the intensity of the UV beam; however, because the GL null is

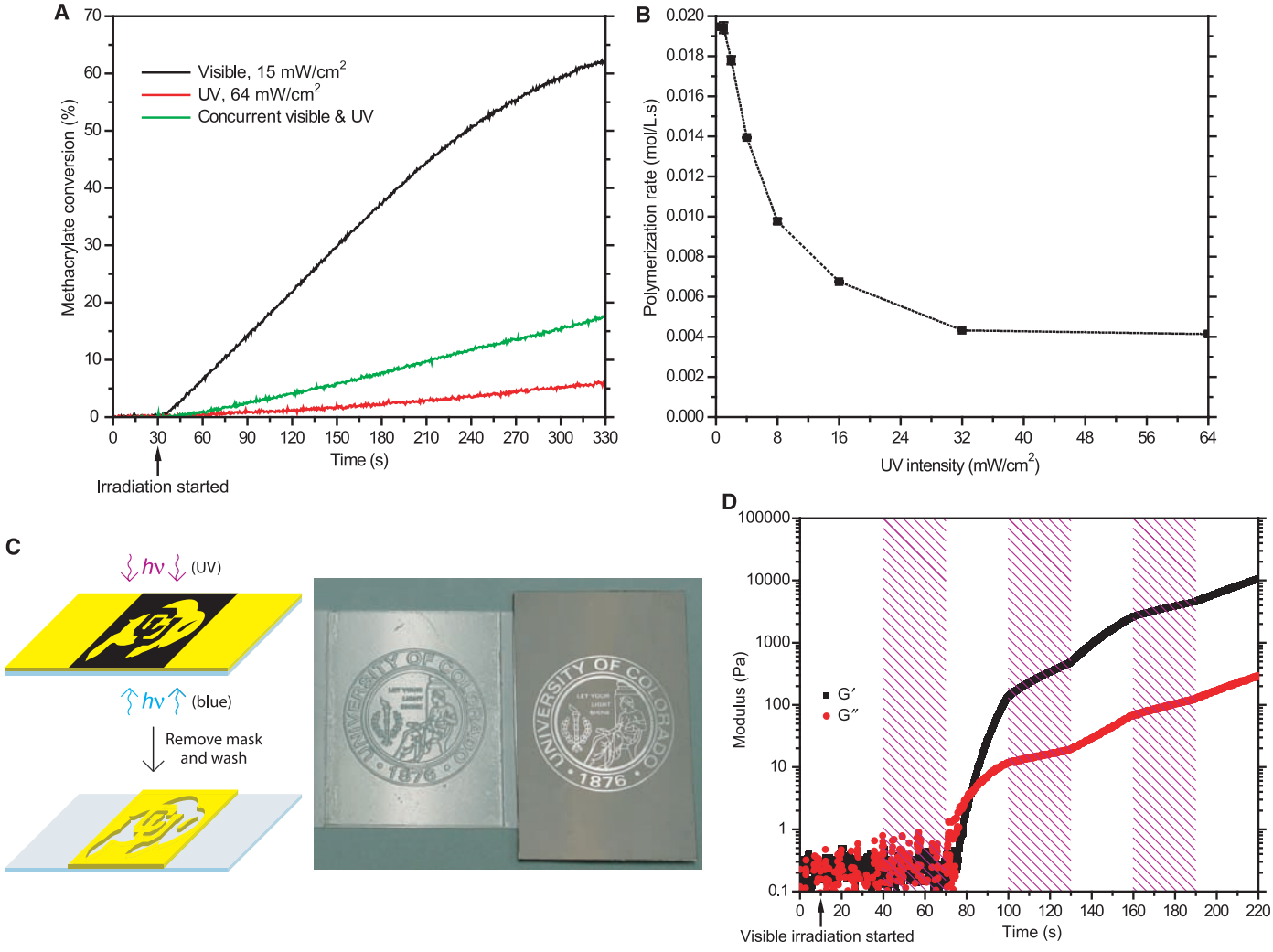

Fig. 3. Effect of photoinhibition on photopolymerization rate. (**A**) Methacrylate conversion profiles for formulated TEGDMA during irradiation. (**B**) Initial methacrylate polymerization rate versus UV irradiation intensity during visible irradiation (15 mW/cm^2). (**C**) Schematic diagram of the photoinitiation-photoinhibition system using mask-based photolithography. A sample produced by using the photoinitiation-photoinhibition system with the photomask used to pattern the photoinhibiting wavelength is also shown. (**D**) Elastic (G′) and viscous (G″) moduli for formulated TEGDMA during constant visible (8 mW/cm^2) and intermittent UV (64 mW/cm^2, indicated by the shaded regions) irradiation.

maintained regardless of intensity, the peak conversion occurring at the center of the focal point is independent of feature width.

The polymerized feature dimensions after removal of ungelled material via solvent wash depend on the degree of monomer conversion past the gelation threshold, as shown in Fig. 1C. Defining a normalized parameter, γ, which equals zero if the center of the feature is just at the conversion to reach gelation and conversely equals one if the entire intensity profile causes gelation, one can predict the polymer feature size for various initiation schemes as a function of peak conversion as shown in Fig. 1D. The one-photon curve defines the diffraction limit; note that this size limit is strongly dependent on the degree of conversion, as shown. The two-photon curve, shown at twice the one-photon wavelength because most two-photon photopolymerization studies are performed with Ti:sapphire lasers at about 800 nm that excite the third-order, nonlinear absorption of an ~400-nm linear absorption, demonstrates that the feature size refinement resulting from two-photon absorption does not compensate for the longer irradiation wavelength. Both single- and two-photon absorption approaches suffer from an inherent trade-off between high conversion and feature size. Conversely, the two-color irradiation scheme used here maintains confinement even at extended irradiation times, enabling the fabrication of features possessing both small size and high, relatively uniform conversions throughout the material; experimental confirmation of this confinement is presented in Materials and Methods.

The monomer, photoinitiator, co-initiator, and photoinhibitor used in this study are shown in Fig. 2, A to D. The monomer, triethylene glycol dimethacrylate (TEGDMA), is readily polymerized to form a cross-linked, gelled polymer via a chain-growth, radical-mediated mechanism. Nonoverlapping absorption bands for the photoinitiator and photoinhibitor allow each of the two irradiating wavelengths to perform their role without encroaching on the role of the other wavelength. Thus, the camphorquinone (CQ)/ethyl 4-(dimethylamino)benzoate (EDAB) visible-light photoinitiation system was chosen in combination with the UV-active tetraethylthiuram disulfide photoinhibitor because camphorquinone does not absorb in the near-UV (Fig. 2E). Blue-light irradiation of TEGDMA formulated with CQ/EDAB and TED excites the photoinitiator (CQ) and initiates the polymerization via carbon-centered radicals, whereas irradiation with UV photocleaves the TED, producing sulfur-centered dithiocarbamyl (DTC) radicals (*16*) that recombine with propagating radicals, end-capping the polymer chain and terminating the polymerization.

Methacrylate conversion profiles during irradiation of the formulated TEGDMA were measured by using time-resolved Fourier transform infrared spectroscopy (Fig. 3A). Whereas the polymerization proceeds rapidly upon irradiation with visible light, UV irradiation generates a very low polymerization rate, both in the presence and the absence of visible-light irradiation. Further, raising the UV intensity during co-irradiation of the resin with both visible and UV monotonically decreases the polymerization rate over the intensity range examined (Fig. 3, A and B), demonstrating effective photoinduced inhibition of the polymerization.

For this system to be translated to photolithography, the reduction in polymerization rate upon UV irradiation needs to be reflected in the time to gelation. The gel point occurs at a critical extent of reaction in a cross-linking system when a single macromolecule first spans the sample and the material transitions from a liquid to a cross-linked, insoluble gel (*17*). This point represents the conversion threshold where ungelled material is still soluble and is readily removed while gelled material remains. The time to gelation for the TEGDMA formulation, as determined by the G′-G″ crossover during parallel-plate rheometry of the material being cured in situ, increased from 50 s for visible irradiation (469 nm, 8 mW/cm^2) to 255 s for simultaneous visible and UV co-irradiation (469 nm, 8 mW/cm^2 and 365 nm, 64 mW/cm^2, respectively). Delayed gelation occurred in regions simultaneously irradiated by visible and near-UV light, whereas gelation occurred more rapidly in regions irradiated exclusively with visible light, enabling facile discrimination between regions exposed to one or both wavelengths. A simple demonstration exploiting this contrast between gela-

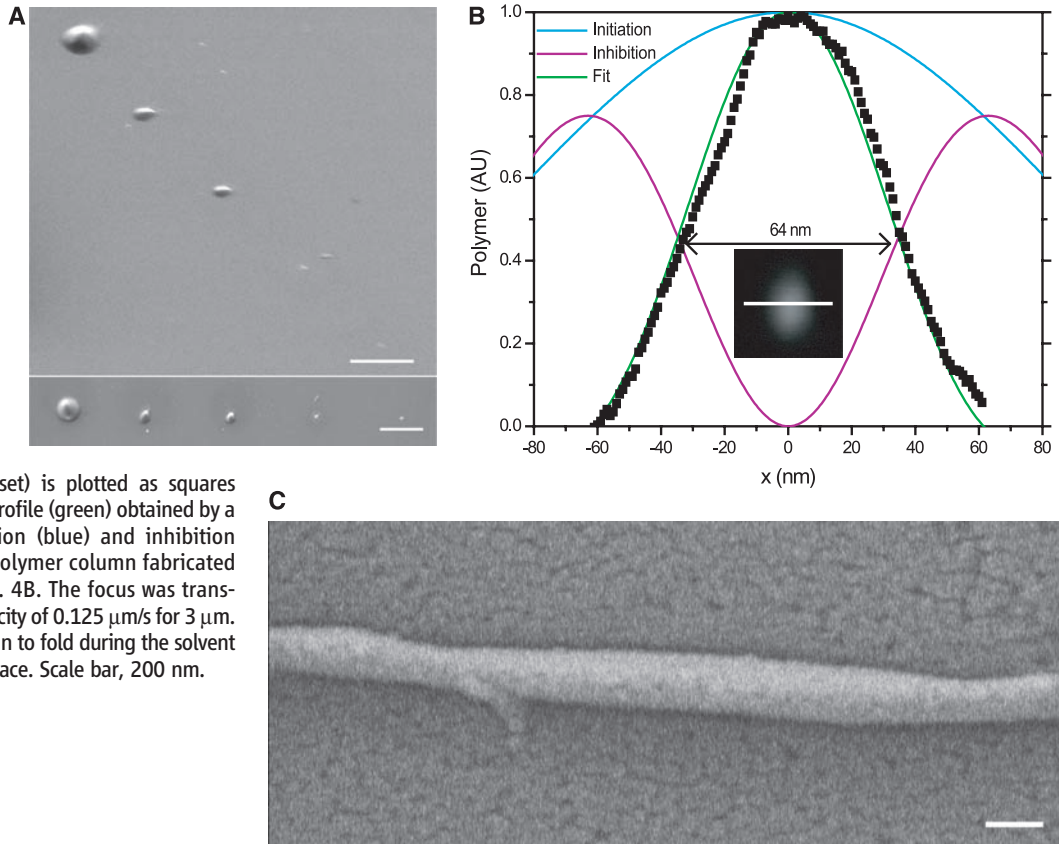

Fig. 4. Scanning electron micrographs of polymerized features. (**A**) Voxels polymerized on a microscope slide using a 0.45-NA singlet lens and the coincident Gaussian blue/GL UV irradiation scheme, observed at 45° and normal to the slide surface. The blue power was held constant at 10 μW while the UV was progressively increased. The UV power, from left to right, was 0, 1, 2.5, 10, and 100 μW. The exposure time was 8 s for each dot. Scale bars, 10 μm. (**B**) Profile of a voxel similarly fabricated but with 10 μW of blue power and 110 μW of UV focused at 1.3 NA, then imaged via SEM at normal incidence. The SEM intensity on the white line (inset) is plotted as squares against the expected polymerization profile (green) obtained by a double-parameter fit of the initiation (blue) and inhibition (violet) rate profiles, as shown. (**C**) Polymer column fabricated by using the same conditions as Fig. 4B. The focus was translated normal to the glass slide at a velocity of 0.125 μm/s for 3 μm. The high aspect ratio caused the column to fold during the solvent wash, leaving it lying on the glass surface. Scale bar, 200 nm.

tion times was performed by using a photomask lithographic approach as shown in Fig. 3C, where resin on a transparent substrate is irradiated uniformly through the substrate with the initiating wavelength while being irradiated by the inhibiting wavelength through a photomask. As a result, the masked region polymerizes and becomes insoluble, whereas the unmasked region remains liquid and is readily washed away.

The fabrication of complex, 3D microstructures requires that the doughnut of inhibiting radicals created spatially to refine the polymerization region be translated in conjunction with the writing spot without leaving a termination trail. This desired behavior in turn requires that the inhibiting species are rapidly eliminated in the absence of the photoinhibition irradiation wavelength. The rapid cessation of photoinhibition in the current system is demonstrated in Fig. 3D. During UV irradiation periods, the polymerization slowed dramatically, as evidenced by the reduced rate of increase in the storage and loss moduli; however, when the UV irradiation ceased, the polymerization rate underwent an immediate and marked increase.

To demonstrate that this polymerization rate control is useful to initiate polymerization below the optical diffraction limit, as predicted by Fig. 1D, we implemented the direct-write lithography scheme shown in Fig. 1A. Polymer voxels were created on a glass substrate and imaged by scanning electron microscopy (SEM) after solvent wash, as shown in Fig. 4A. As predicted in Fig. 1D, increasing the UV power, and therefore the photoinhibition rate, of the GL mode progressively reduces the voxel diameter in a controllable manner. In the sequence shown, the constant-power, 1.3-μm (full width to $1/e^2$) blue focus has written polymer voxels with diameter varying from 3.6 μm with no UV down to 200 nm for strong UV inhibition at 100 μW UV irradiation power. This resolution is typical of two-photon initiation using ~1.4 numerical aperture (NA) lenses (*2*, *5*) with aberration-limited depth ranges of tens of μm; the much lower NA demonstrated here enables mm-scale thicknesses. In Fig. 4B we show the ability to create 110-nm voxels full width and 65 nm full width at half maximum by using a 1.3-NA lens and measured by SEM, approaching the size of the smallest features produced with use of two-photon photopolymerization (*6*). Continuous writing under these conditions with the superimposed Gaussian/GL irradiation scheme is shown in Fig. 4C, resulting in lines of similar diameter. Reduction of voxel diameters using this irradiation scheme could be effected in other materials such as those containing reversibly photodimerizable functionalities, where dimers are created by irradiation at one wavelength and cleaved by irradiation at a different wavelength; however, photoreversibility precludes translation of a writing spot and disallows fabrication of dense, 3D structures.

Two-photon photopolymerization has been described as the only microprocessing approach with intrinsic 3D fabrication capability (*18*). Although the optical approach demonstrated here produces confinement of the polymerized region along only two axes, manipulation of the photoinhibiting wavelength into a bottle beam profile (*19*) would induce confinement along the third axis, thus allowing fabrication of 3D structures with sub–100-nm isotropic resolution. Because single-photon absorption cross sections are often orders of magnitude larger than two-photon cross sections, this photoinitiation-photoinhibition system facilitates the use of inexpensive continuous wave (CW) diode lasers and very high write velocities. Thus, this single-photon approach to nanolithography uses dramatically cheaper hardware and scales to much higher throughput.

References and Notes

1. A. C. Sullivan, M. W. Grabowski, R. R. McLeod, *Appl. Opt.* **46**, 295 (2007).
2. S. Kawata, H.-B. Sun, T. Tanaka, K. Takada, *Nature* **412**, 697 (2001).
3. B. H. Cumpston *et al.*, *Nature* **398**, 51 (1999).
4. H.-B. Sun *et al.*, *Opt. Lett.* **25**, 1110 (2000).
5. T. Tanaka, H.-B. Sun, S. Kawata, *Appl. Phys. Lett.* **80**, 312 (2002).
6. W. Haske *et al.*, *Opt. Express* **15**, 3426 (2007).
7. N. C. Strandwitz *et al.*, *J. Am. Chem. Soc.* **130**, 8280 (2008).
8. K. Ichimura, M. Sakuragi, *J. Polym. Sci. Polym. Lett. Ed.* **26**, 185 (1988).
9. S.-K. Lee, D. C. Neckers, *Chem. Mater.* **3**, 852 (1991).
10. S.-K. Lee, D. C. Neckers, *Chem. Mater.* **3**, 858 (1991).
11. D. J. Lougnot, D. Ritzenthaler, C. Carre, J. P. Fouassier, *J. Appl. Phys.* **63**, 4841 (1988).
12. S. K. Soh, D. C. Sundberg, *J. Polym. Sci. Polym. Chem. Ed.* **20**, 1299 (1982).
13. G. Donnert *et al.*, *Proc. Natl. Acad. Sci. U.S.A.* **103**, 11440 (2006).
14. Materials and methods and a study examining the effect of exposure time on polymerized feature size are detailed in supporting material available on *Science* Online.
15. P. J. Flory, in *Principles of Polymer Chemistry* (Cornell Univ. Press, Ithaca, NY, 1953).
16. L. G. Lovell, B. J. Elliott, J. R. Brown, C. N. Bowman, *Polymer* **42**, 421 (2001).
17. F. Chambon, H. H. Winter, *J. Rheol.* **31**, 683 (1987).
18. H. B. Sun, S. Kawata, in *NMR - 3D Analysis - Photopolymerization* (Springer, Berlin, 2004), vol. 170, pp. 169–273.
19. J. Arlt, M. J. Padgett, *Opt. Lett.* **25**, 191 (2000).

20. Supported by NSF programs IIP-0750506, IIP-0822695, and ECS-0636650, NIH grant DE10959, and the University of Colorado Innovative Seed Grant Program. A preliminary patent based on this technology has been filed by T.F.S., A.C.S., C.N.B., and R.R.M.

Supporting Online Material

www.sciencemag.org/cgi/content/full/1167610/DC1
Materials and Methods
Fig. S1
References

23 October 2008; accepted 24 March 2009
Published online 9 April 2009;
10.1126/science.1167610
Include this information when citing this paper.

Confining Light to Deep Subwavelength Dimensions to Enable Optical Nanopatterning

Trisha L. Andrew,[1] Hsin-Yu Tsai,[2,3] Rajesh Menon[3,4]*

In the past, the formation of microscale patterns in the far field by light has been diffractively limited in resolution to roughly half the wavelength of the radiation used. Here, we demonstrate lines with an average width of 36 nanometers (nm), about one-tenth the illuminating wavelength λ_1 = 325 nm, made by applying a film of thermally stable photochromic molecules above the photoresist. Simultaneous irradiation of a second wavelength, λ_2 = 633 nm, renders the film opaque to the writing beam except at nodal sites, which let through a spatially constrained segment of incident λ_1 light, allowing subdiffractional patterning. The same experiment also demonstrates a patterning of periodic lines whose widths are about one-tenth their period, which is far smaller than what has been thought to be lithographically possible.

Optical patterning is the primary enabler of microscale devices. However, the Achilles heel of optics is resolution. The far-field diffraction barrier limits the resolution of optical systems to approximately half the wavelength (*1*) and therefore restricts nanoscale patterning at visible wavelengths. Scanning electron beam patterning has thus become the preferred method for fabricating nanostructures. However, electrons are affected by extraneous electromagnetic fields, limiting the accuracy with which patterns can be placed relative to one another (*2*). Furthermore, electron flux is limited by mutual repulsion effects, constraining the patterning speed (*3*). The vacuum environment and electron lenses increase system complexity and cost. Alternatively, the diffraction barrier can be overcome in the optical

[1]Department of Chemistry, Massachusetts Institute of Technology (MIT), Cambridge, MA 02139, USA. [2]Department of Electrical Engineering and Computer Science, MIT, Cambridge, MA 02139, USA. [3]Research Laboratory of Electronics, MIT, Cambridge, MA 02139, USA. [4]LumArray, Somerville, MA 02143, USA.

*To whom correspondence should be addressed. E-mail: rmenon@mit.edu